chemosensors

MDPI

Article

Sulfide Detection by Gold-Amalgam Microelectrodes in Artificial Wastewater

Jonas M. S. Andrich * and Uwe Schröder *

Institute of Environmental and Sustainable Chemistry, Technische Universität Braunschweig, Hagenring 30, 38106 Braunschweig, Germany

* Correspondence: Jonas.Andrich@gmail.com (J.M.S.A.); uwe.schroeder@tu-braunschweig.de (U.S.)

Received: 14 May 2020; Accepted: 30 June 2020; Published: 2 July 2020



Abstract: Gold amalgam microelectrodes (GAMEs) have been characterized and successfully calibrated to measure >1.5 mM (30 mg L^{-1}) sulfide in artificial wastewater (AWW) using cathodic stripping voltammetry (CSV). Microbial sulfide generation in two types of AWW was traced. Artificial wastewater type 1 (AWW1) held the potential for almost 50% conversion of sulfur compounds at a maximum rate of ~4.3 ± 0.5 µM h^{-1} while AWW 2 held a potential for 75–100% conversion at a rate of 165 µM h^{-1}. In addition, the GAMEs were thoroughly examined during fabrication, maturation, and aging. An earlier described plating method was found to result in varying electrode surfaces due to excess mercury deposition and, therefore, deviating stripping signals. The limited shelf life of GAMEs has been proposed previously. This study shows the extent of electrode surface changes during amalgam formation and the wear and tear of application. As a result, suggestions to optimize fabrication and application are discussed to provide reliable measurements and proceed toward a future commercialization.

Keywords: sulfide; cathodic stripping voltammetry; electroanalysis; microelectrode; online sulfide detection; artificial wastewater; solid state microelectrode; gold amalgam; microbial fuel cells

1. Introduction

Sulfide emissions in the sewer are undesired. They cause corrosion, spread an unpleasant scent, and endanger the operators [1,2]. They originate mostly from microbial dissimilatory sulfate conversion or the degradation of other sulfurous compounds such as cysteine [3,4]. Unfortunately, the methods to prevent sulfide emissions are often discontinuous and, therefore, less efficient [5,6]. Online sulfide detection increases the efficiency of these methods as it allows taking action in the right place and time.

Ways to detect sulfide are manifold [7]. One of them is cathodic stripping voltammetry (CSV) using gold amalgam microelectrodes (GAMEs). This electroanalytical method has already been used for the online detection of sulfide in the sea and freshwater [8–12]. The principle is beneficial for several reasons. The amalgam has a high hydrogen overpotential and allows, therefore, to detect analytes with low redox potential without interfering hydrogen evolution. Solid amalgam is mechanically more stable compared to classical mercury drop electrodes. The microelectrode allows sharp peaks due to a reduced ratio between capacitive and faradaic currents. Lastly, the electrode fabrication is cheap and convenient.

Despite these benefits, GAMEs have not been adapted for use in wastewater. This may be due to wastewater's complex and chemically-challenging sample matrix. Being only partially selective for analytes, CSV might be prone to interferences [12]. According to van den Berg in general, there are three potential types of potential CSV interferences: (i) competitive adsorption of species, (ii) competitive absorption of surface active organic compounds, and (iii) competition by complexing ligands present in

the sample. Surface-active organics such as surfactants [13] and ligands are also present in wastewater, which might result in completion for adsorption [14].

The primary scope of this study was to adapt the gold amalgam microelectrode cathodic stripping voltammetry (GAME CSV) to the complex sample matrix of the microbial environment of wastewater. This was attempted by using complex but defined media mimicking sewage for the application in microbial fuel cells [15], which is known as artificial wastewater (AWW).

The gold amalgam electrode were made simply by mercury plating on top of a polished gold surface [8,10,11,16–20]. The amalgam forms upon diffusion of gold into the plated mercury and vice versa. It starts to crystallize as gold enriches above 0.13% (w_{Au}/w_{Hg}). As long as the gold-mercury-amalgam system is not in equilibrium, its thickness, chemical composition, and microstructure will change over time [21]. These temporal changes are meaningful for electrode application and will be discussed later.

Although the steps of solid amalgam electrode fabrication are well described [8,17], and it is known that the electrodes have a limited shelf life, the surface changes are less well documented. For instance, Bobrowski and Królicka refer to an unpublished observation by Bás of support metals affecting the overlaying mercury film [21].

In summary, the goal of this study was to develop a robust electroanalytical method for the online-detection of sulfide emission in complex media based on gold amalgam electrodes. The analytical method was intended to trace the microbial sulfide emission of anode respiring bacteria in the context of microbial fuel cell research for energy harvesting from wastewater.

2. Materials and Methods

2.1. Gold Amalgam Microelectrode

A 100-µm gold wire was placed in a glass capillary. The capillary was filled with epoxy (Epoxy resin L and hardener GL 2, R&G GmbH) and hardened for 2 days at 90 °C to achieve glass transition. The electrode was subsequently soldered to a 2-mm banana jack and was ground and polished with circular motions for one minute at each step. First, sanding paper was used in the following order: P240, P400, and P600. Then micro-mesh polishing cloth was used in the following order: 1500, 1800, 2400, 3200, 4000, 6000, 8000, and 12,000, and then 1-µm monocrystalline diamond particles (MetaDi II, Buehler) on a hard polishing cloth (TexMet C, Buehler) and 0.25-µm monocrystalline diamond particles (MetaDi II, Buehler) on a soft polishing cloth (MicroCloth, Buehler). Between the steps and after polishing, the electrode was cleaned with isopropanol and water and, afterward, dried by pressure air to avoid displacement of grinding material. Photographic images of the electrode are shown in Figure S1 in the Supplementary information.

The polished gold electrode was plated with mercury for 4 min at a potential of −100 mV vs. Ag/AgCl (SE11, Meinsberger) in a 100 mL 0.1 M $Hg(NO_3)_2$ of pH 1.5 at room temperature [8]. The solution was continuously stirred and sparged with nitrogen to maintain oxygen-free conditions. As soon as the mercury was plated, amalgam formation proceeds (Figure 1a–c).

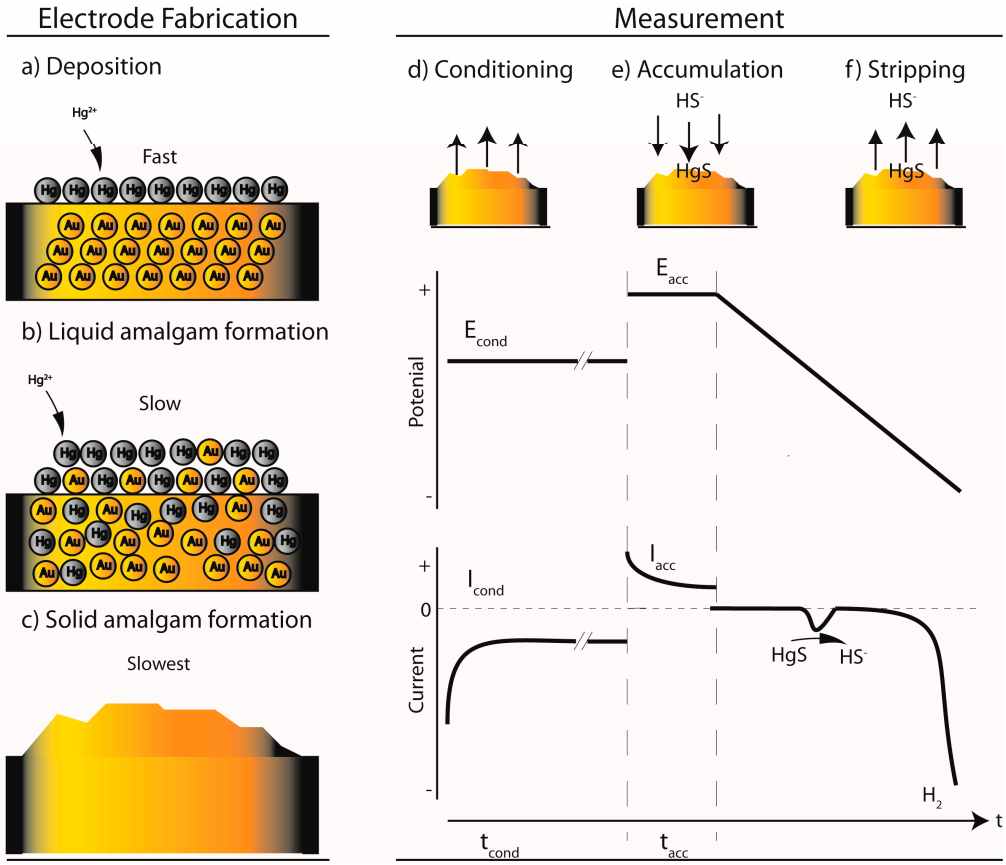


Figure 1. Scheme of gold amalgam formation (**a**–**c**) and cathodic stripping voltammetry (**d**). Mercury (Hg) deposition on polished gold (Au). (**b**) Diffusion of gold into mercury-forming liquid amalgam and vice versa. (**c**) Solid gold amalgam formation through crystallization. (**d**) Conditioning potential E_{cond} is applied for t_{cond}. (**e**)The accumulation potential E_{acc} is applied for t_{acc}. (**f**) Lastly, a cathodic sweep is performed at a speed v_{sweep}. Its current wave peak is proportional to the analyte concentration according to the Randles-Sevcik equation [22]. Sulfide peak was expected at potentials below −0.6 V vs. Ag/AgCl.

2.2. Cathodic Stripping Voltammetry

Cathodic stripping voltammetry (CSV) is a three-step process (Figure 1d–f). First, a conditioning potential E_{cond} of −0.9 V vs. Ag/AgCl was applied for t_{cond} of 5 s to maintain a clean electrode surface (Figure 1d). Second, a deposition potential E_{acc} of −0.1 V was held for t_{acc} of 2 s to enrich sulfide as HgS on the amalgam electrode (Figure 1e).

$$HS^- + Hg \rightarrow HgS + H^+ + 2\,e^- \quad (1)$$

Third, a cathodic sweep (Figure 1f) was performed at a speed v_{sweep} of 2 V/s with a start and end potential E_i of −0.1 V and a vertex potential E_1 of −1.8 V. At −0.6 V vs. Ag/AgCl sulfide is stripped from the electrode.

$$HgS + H^+ + 2\,e^- \rightarrow HS^- + Hg. \quad (2)$$

All experiments were performed in a Faraday cage or with shielded electrodes to avoid inductive interferences.

2.3. Calibration and Measurement

Sulfide calibration and quantitative determination measurements were performed at room temperature under oxygen-free (anaerobic) conditions to prevent oxidation side products. Sodium

sulfide ($Na_2S \cdot 9H_2O$) was washed with deionized water and dried prior to use to minimize interfering oxidation products during the measurement [23]. The sulfide stripping peaks were determined by the Gaussian quick peak fit function of OriginLab®. The region of interest (ROI) was set to −0.4 to −0.9 V vs. Ag/AgCl. The baseline set by the starting point of the CSV forward sweep. This approximation allowed us to handle large datasets in a short amount of time.

The methylene blue method (MB) was used as a reference method to compare CSV-determined sulfide concentrations spectrophotometrically at 670 nm (see also dilution series depicted in Figure S2). The method of Cline [24] was adapted by scaling down the sample size to 5 mL.

2.4. Media and Cultivation

Two types of artificial wastewater were used, which have been described and compared earlier by Riedl et al. [25]. Type 1 artificial wastewater is frequently used in microbial fuel cell research to cultivate electrochemically active (current producing) bacterial biofilms [15,26] and type 2 artificial wastewater has been developed recently [25]. Type 1 artificial wastewater (AWW 1) consisted of neutral 50 mM phosphate buffer supplemented with 10 mM acetate as a sole carbon source [15,27]. Its total atomic sulfur content was 212 µM. On the opposite, artificial wastewater of the second type (AWW 2) had a sulfur content of 2212 µM. It was based on carbonate buffer containing 6 µM ammonium chloride, 2 µM potassium chloride, 10 mM sodium bicarbonate, 10 µM sodium carbonate, 1.29 mM monosodium phosphate, and is more diverse in its carbon sources. It was supplemented with 0.67 mM potassium hydrogen phthalate, 2.5 mM sodium acetate, 0.42 mM glucose, 0.5 mM D-ribose, 3.33 mM glycine, and 2 mM cysteine. Both types of AWW were supplemented with 12.5 mL L^{-1} vitamin and 12.5 mL L^{-1} trace element solution [15,28]. The trace element solution contained 7.85 mM nitrilotriacetic acid, 12.17 mM magnesium sulfate, 2.67 mM manganese(II) sulfate, 17.11 mM sodium chloride, 0.36 mM iron(II) sulfate, 0.77 mM cobalt(II) chloride, 0.68 mM calcium chloride, 0.62 mM zinc sulfate, 40 µM copper(II) sulfate, 40 µM potassium aluminium sulfate, 0.16 mM boric acid, and 50 mM sodium molybdate. The media were inoculated with 1 mL of wastewater for anaerobic cultivation at room temperature in 250-mL batches.

2.5. Confocal Laser Scanning Microscopy (CLSM)

CLSM images were taken with a Leica TCS SPE confocal laser scanning microscope equipped with a HC PL FLUOTAR 50×/0.80 DRY microscope objective at 500× magnification. A blue laser (480 nm) was used at low intensity (5–15%) to scan the sample with a gain of 400 and 0% offset at 400 Hz. The images were taken at a resolution of 1024 × 1024 pixels reflecting a 220 µm × 220 µm sample area. Thus, one pixel represented 215 nm × 215 nm. The pinhole was set to 0.5 airy units. The z-stack slice height was less than 1 µm. Planar electrode projections of the top view or side-view were created using the re-slice and the z-stack projection feature of FIJJI [29].

3. Results

3.1. Temperature and Accumulation Time Influence Stripping Signals

Temperature influences diffusion coefficients and reaction rates and, therefore, the analyte accumulation and stripping peak current. The first experiment was performed to estimate the temperature influence on the cathodic stripping peak of sulfide. For this purpose, the temperature was changed at a constant sulfide concentration of 25 µM (Figure 2a). It was found that the sulfide stripping peak current I_P depends linearly on the temperature in the tested range.

$$I_p(T) = \vartheta^* a_{cor} + b \quad (3)$$

where ϑ is the temperature [°C], a_{cor} is a correlation factor [nA/°C], and b is the signal baseline [nA]. For 25 µM sulfide, a_{cor} was found at 32 ± 2 nA/°C. Increasing the temperature by 1 °C at room

temperature would lead to a signal drift of 30% and a respective overestimation of sulfide in the system. This indicates a strong temperature influence, especially at room temperature.

Another key parameter influencing the stripping peak height and determining sensitivity is the accumulation time, t_{acc}. Its impact on stripping peak height was determined by varying t_{acc} from 2 to 60 s at a constant sulfide concentration (Figure 2b).

The peak height I_p and accumulation time correlated well in a quadratic manner ($R^2 \sim 1$). The response was linear up to ~ t_{acc} = 20 s and declined beyond indicating saturation effects. Accordingly, t_{acc} was set to two seconds to obtain a linear signal response. Theoretically, the adjustment of t_{acc} allows a dynamic linear signal range during online measurements.

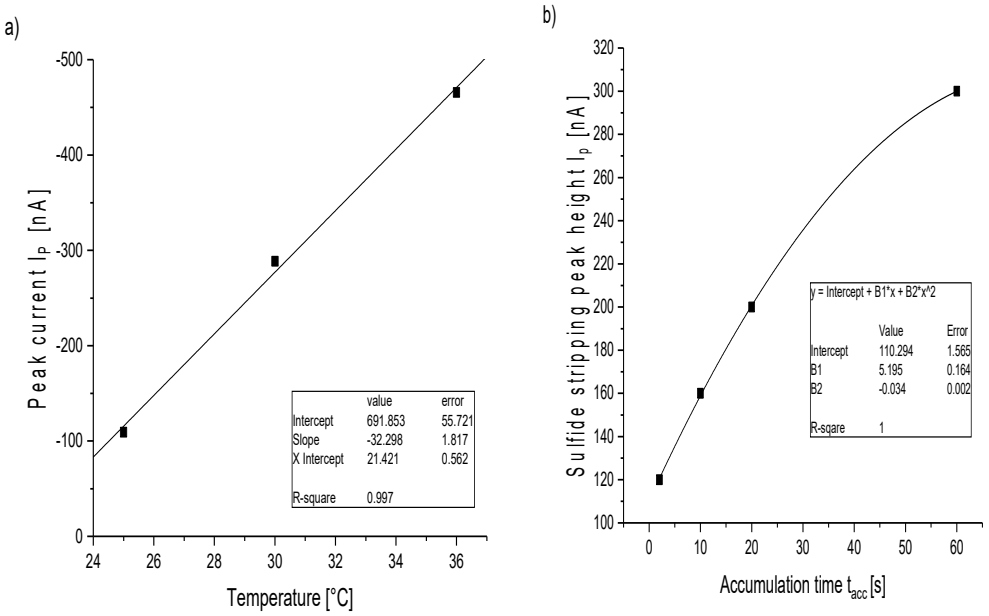


Figure 2. Stripping peak current I_p effected by (**a**) temperature and (**b**) by accumulation time t_{acc}. AWW 1 with 25-µM sulfide.

3.2. GAME Calibration in AWW 1

Based on its composition (sulfur-containing compounds), AWW 1 holds the potential for a maximum sulfide formation of ~200 µM. We tested whether a linear signal response could be obtained for CVS within this range (Figure 3a).

The sulfide peak heights correlated well with the sulfide concentration over the whole range with an R^2 of 0.98 (Figure 3b). In addition, a measurement comparing pure phosphate buffer and AWW 1 indicated little initial interferences between media composition and sulfide measurements (Figure S3 in the Supplementary information). Neither reduction peaks of Mn^{2+} nor Zn^{2+}-were visible despite being present in AWW 1 at concentrations of 33 and 8 µM, respectively. The previously suggested minimum detection limit from Luther et al. [8] of about 5 µM for Mn^{2+} and below 0.1 µM for Zn^{2+} using square wave voltammetry could not be reached under our experimental conditions and by using linear cathodic sweeps.

3.3. Tracing Microbial Sulfide Formation in AWW 1

After calibration, it was tested if the CSV-GAME method was suitable for the real-time detection of sulfide over an extended period. For this purpose, CSV was performed in wastewater inoculated AWW 1 every half hour over four days (Figure 4a).

Using CSV, sulfide stripping peaks became visible after 20 h and then steeply increased to a maximum at 42 h. Afterward, during a gradual decline, the peak currents oscillated (Figure 4a). It was not clear whether the oscillation originated partially from real fluctuations of sulfide concentrations or

solely from the CSV method. The MB and CSV calibrations were used to determine the respective sulfide concentration (Figure 4b). The quantities and rates of sulfide emission determined by CSV were in good agreement with those estimated with Methylene Blue (Figure 4, MB1–MB3). Notably, the lag time for sulfide emission varied broadly between measurements, which ranged from 10 to 50 h.

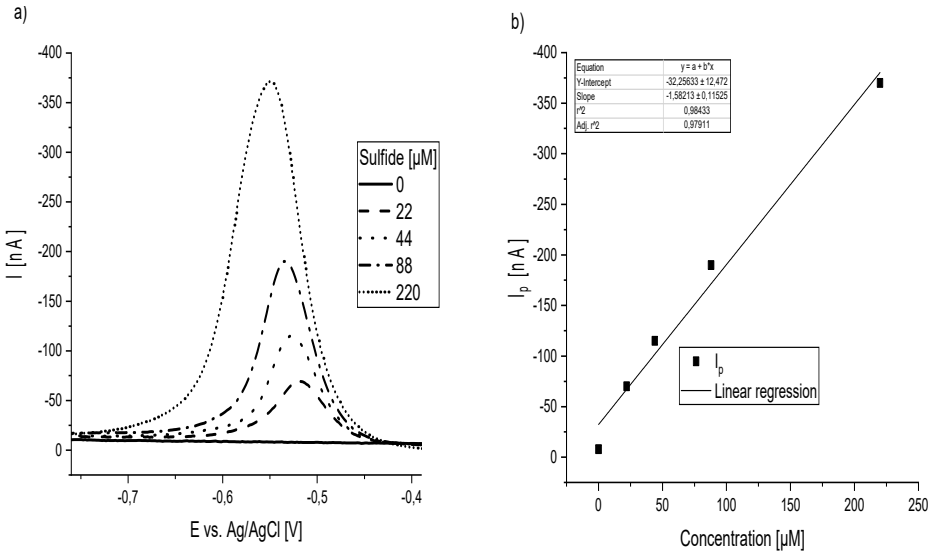


Figure 3. (**a**) Voltammograms of cathodic stripping during GAME calibration and (**b**) respective sulfide calibration curve in type 1 artificial wastewater (AWW 1) at room temperature.

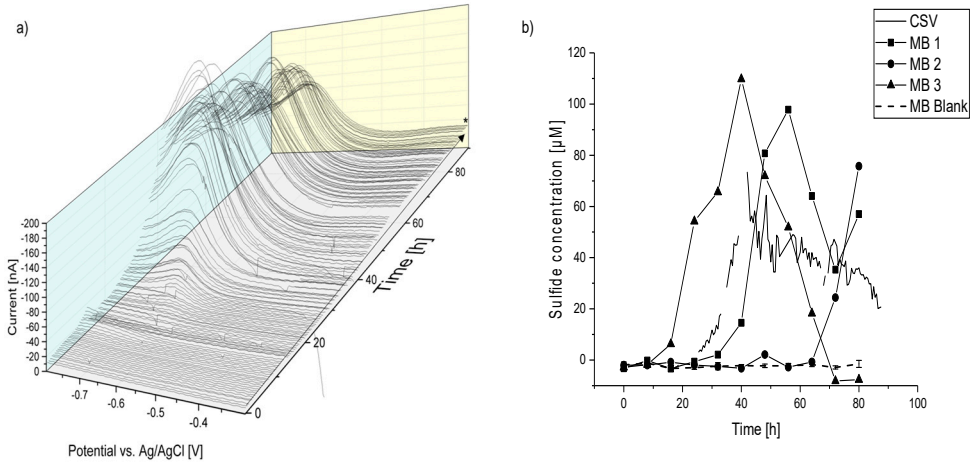


Figure 4. Microbial sulfide emission in AWW 1 over time. (**a**) Cathodic sweeps with stripping peaks. (**b**) Derived sulfide concentrations by cathodic stripping voltammetry (CSV) and the Methylene Blue method.

The maximum sulfide concentration of 90 ± 17 µM represented nearly half of the potential 200 µM. This indicates either partial sulfate conversion, further sulfide reaction, or sulfide that left the system. The maximum sulfide formation rate was 4.3 ± 0.5 µM h^{-1}.

3.4. GAME Calibration in AWW 2

Artificial wastewater 2 is more diverse in terms of organic carbon content and intended to represent real wastewater more accurately. It has a higher inherent capacity for sulfide formation. Cysteine and sulfate conversion might yield a total of 2212 µM sulfide. Therefore, it was tested if a linear GAME CSV response could be obtained within the possible concentration regime of AWW 2 (Figure 5b).

The stripping peak height correlated well with sulfide concentrations ranging from 50 to 500 µM (Figure 5a). In contrast to the previous experiment with AWW 1, peaks became only visible above a sulfide threshold of ~50 µM (Figure 5a, inset). These effects might be due to the removal of sulfide by metal precipitation in the slightly more alkaline environment of AWW 2. Above a sulfide concentration of 1500 µM, saturation effects became visible. A second more cathodic peak appeared when sulfide exceeded a concentration of 415 µM (Figure 5b). Since there was no associated oxidative peak in the back scan (data not shown), a non-reversible reaction was assumed. This might be associated with the flattening of the calibration curve, which will be later discussed.

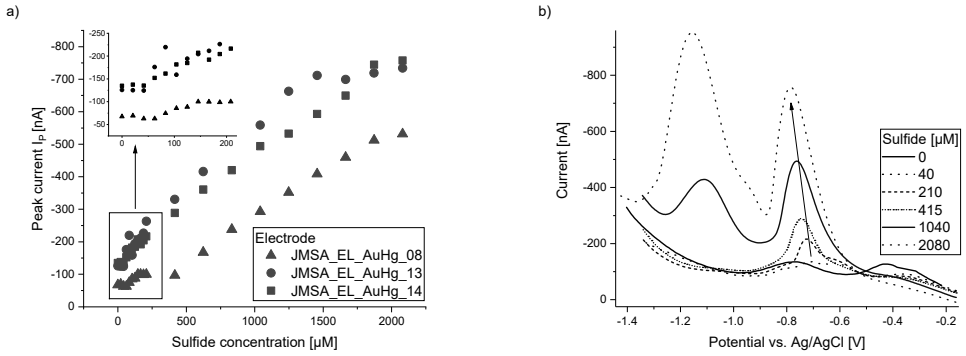


Figure 5. (**a**) Sulfide calibration with three different gold amalgam microelectrodes with the electrode identifiers JMSA_EL_AuHg_08, JMSA_EL_AuHg_13, and JMSA_EL_AuHg_14 (100-µm electrode surface diameter each) and (**b**) selected forward sweeps in sterile AWW 2 at room temperature.

3.5. Tracing Microbial Sulfide Formation in AWW 2

Once the GAME was calibrated, it was used to trace sulfide emissions in AWW 2. The final concentrations were compared using the Methylene Blue method as a reference.

The sulfide emission exhibited a sigmoidal course with a lag phase, exponential increase, and subsequent decay. This is a typical course for microbial growth associated with product formation in batch processes (straight line, Figure 6). The lag phase was 10 h and the exponential phase was between 15 h and 25 h. Sulfide decrease took place after 30 h. The final average concentration derived by methylene blue was lower when compared to the CSV result by approximately 500 µM. The maximum calculated sulfide conversion rate was 165 µM h^{-1}, which is >30 times higher than for AWW 1. Over time, 75–100% of sulfuric compounds were converted to sulfide. The lag phase was less variable when compared to AWW 1.

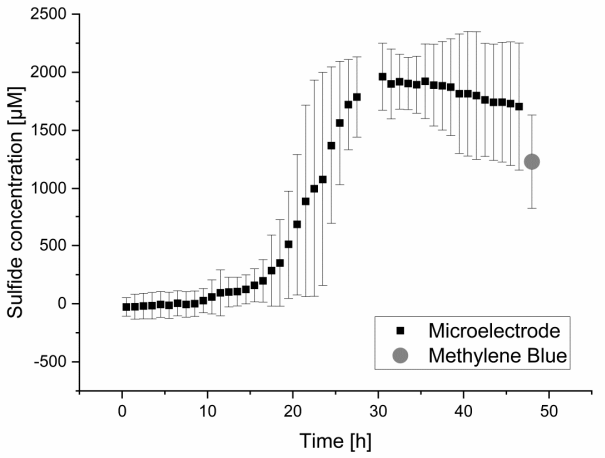


Figure 6. Microbial sulfide emission in AWW 2 at RT traced by gold amalgam microelectrodes (GAME) and the Methylene Blue method (for six separately performed replicate experiments).

3.6. GAME Stability during Operation

GAMEs are known for their limited shelf life. It was assumed that a stable amalgam electrode would give stable I_{cond} and I_{acc} over time. Therefore, these parameters were regarded as quality indicators. They were determined while repeatedly performing CSVs during the previous biological sulfide emission tests in AWW 2 (Figure 7a).

The figure aggregates several hundred CSV cycles throughout a six-day measurement and approximately 85,000 data points. This large dataset contains two pieces of information. First, Figure 7a illustrates the general current response trend during accumulation (top, oxidative) and conditioning (bottom, reductive). It represents the order of magnitude of the current response. During the initial microbial growth, the conditioning currents increased. As soon as the sulfide production sets in, also the accumulation currents increased. A potential cause for later current variations might be microbial (secondary) metabolite production or lysis products.

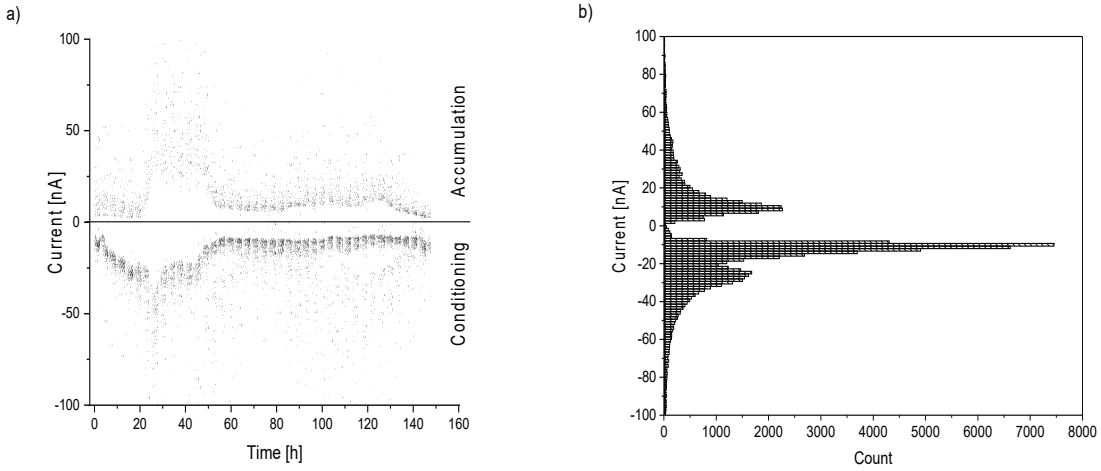


Figure 7. (**a**) Accumulation ($I_{acc} > 0$) and conditioning current ($I_{cond} < 0$) for six days of continuous CSV to measure microbial sulfide emission. AWW 2 at room temperature with $E_{cond} = -0.9$ V, $t_{cond} = 5$ s, $E_{acc} = -0.1$ V vs. Ag/AgCl and $t_{acc} = 2$ s. Every 30 min, four consecutive cycles were performed and 10 data points per second were recorded. (**b**) Histogram of accumulation and condition current to illustrate the distribution of data points of time series in (**a**).

Second, the histogram in Figure 7b indicated that the current of the conditioning step is likely to remain in the regime above −20 nA. This stable reductive current implies that the electrode surface has not been subject to severe deterioration. Such a deterioration would have led to higher hydrogen reduction rates either by gold exposure or changes in electrode composition and reduced hydrogen onset, which both lead to increased reductive currents.

In summary, a GAME could be operated for CSV online sulfide determination in complex AWW 2 environments for at least six days.

3.7. Variability of Deposition Procedure and Its Impact on Calibration

For applications beyond fundamental research, a reliable electrode production process is desired. Therefore, the proposed deposition method was examined for reproducible mercury plating. For this purpose, the plating charge of the mercury deposition was compared among several fabricated electrodes (Figure 8).

The plating charge varied broadly, which ranged from a few millicoulomb up to above 200 mC. In a previous study, it was found that 10–20 µm deposition height was sufficient to maintain proper electrode function during CSV [8]. This required only plating mercury equivalent to 2 mC. From these results, it can be concluded that the required charge was exceeded most of the time, which presumably resulted in a higher deposition.

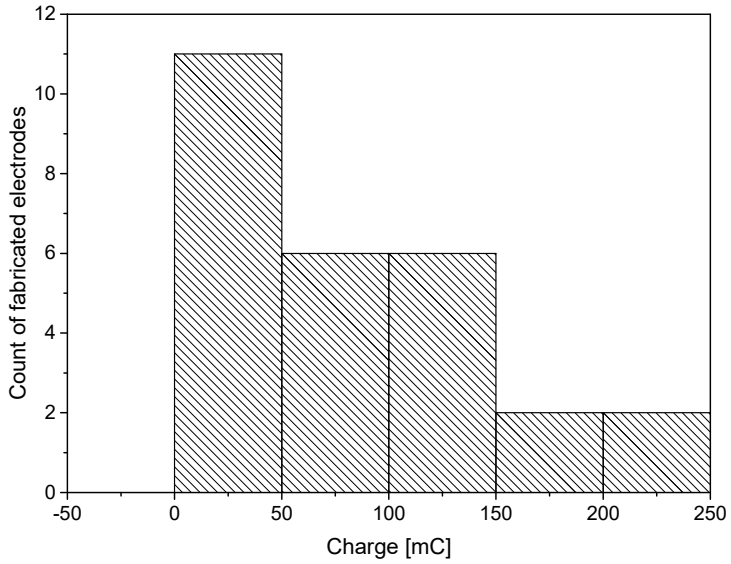


Figure 8. Variability in mercury plating charge during fabrication of gold amalgam microelectrodes (n = 27).

The resulting shapes and heights of the deposited mercury were further investigated. For this purpose, the plating charge was correlated with the visible mercury deposition using confocal laser scanning microscopy (Figure 9a–e).

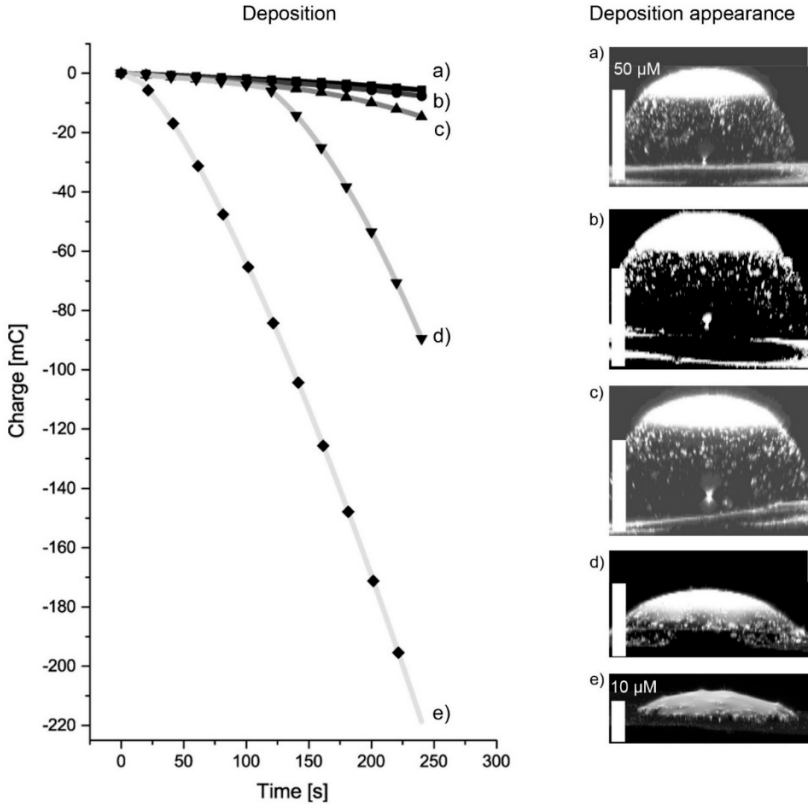


Figure 9. Mercury-deposition charge and resulting deposition appearance for five representative GAMEs. All gold electrodes were 100 µm in diameter, polished and plated with mercury as described in the method section. The electrodes (**a**–**e**) have the electrode identifiers JMSA_EL_AuHg_17, JMSA_EL_AuHg_20, JMSA_EL_AuHg_19, JMSA_EL_AuHg_18, and JMSA_EL_AuHg_21, respectively. The white bar represents 50 µm unless otherwise specified.

The visible depositions appeared thicker than the expected 10–20 µm (Figure 9a–c). The cone-shaped depositions reached up to a maximum height of approximately 80 µm. Thus, more mercury than required was plated.

High amounts of plating charge did not correlate well with large depositions. For electrodes (a), (b), and (c) charge and visible height were in accordance, but, in contrast, electrodes (d) and (e) showed only small visible depositions despite high amounts of plating charge.

In summary, the plating strategy resulted in different electrode sizes and shapes. The resulting variable electrode surface will influence cathodic stripping signals. To determine the extent, the sulfide stripping response during calibration was tested for three different representative electrode shapes (Figure 10).

The sulfide stripping peak current at a respective concentration was dependent on the electrode geometry. With increased deposition height and a potentially larger surface area, the stripping current increases. At above 200 µM sulfide concentration, the largest electrode resulted in two times the peak height as compared to the flat electrode.

Given these results, the applied method for mercury deposition was found to have potential for improvements if reproducible electrode sizes are desired.

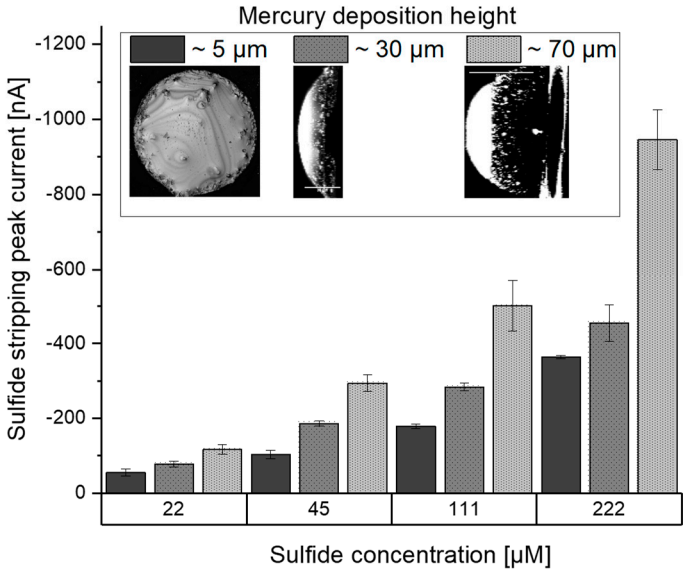


Figure 10. Electrode response during sulfide calibration for varying mercury deposition heights. Twelve consecutive measurements at a certain sulfide concentration with each electrode were performed.

3.8. GAME Maturation and Aging

A defined electrode surface area is desired for reproducible electroanalytical measurements. The electrode surface of gold amalgam electrodes may change over time, but little is known about its extent. Therefore, the temporal changes of the surface structure were examined qualitatively by confocal laser scanning microscopy. Two types of gold amalgam microelectrodes were considered including one with an initial thin mercury film deposition (Figure 11) and one with a large spherical deposition (Figure 12).

For the flat structure, right after mercury plating, several crystallization nuclei became visible. They were visible at the boundary region of the circular electrode and within the liquid mercury. They grew and propagated quickly across the surface while the liquid mercury gradually disappeared. After 5 h, nearly all liquid mercury disappeared. The crystal shapes were heterogeneous and do not conform with the ideal cubic, rhombic, and icosahedra geometries observed in previous experiments [30] or in the field [31].

After 1 h and 40 CV cycles in plain phosphate buffer, the surface did not further change profoundly. In contrast, after 48 h, a sulfide calibration occurred and, after further measurements, the surface roughened visibly. In addition to the roughening, some crystal structures partially merged together and appeared to bloat (lower right region of the electrode). It is not clear whether the change is due to the ongoing crystallization or interaction with the analyte and buffer. In contrast to flat depositions, large spherical plating resulted in a single monolithic crystal (Figure 12).

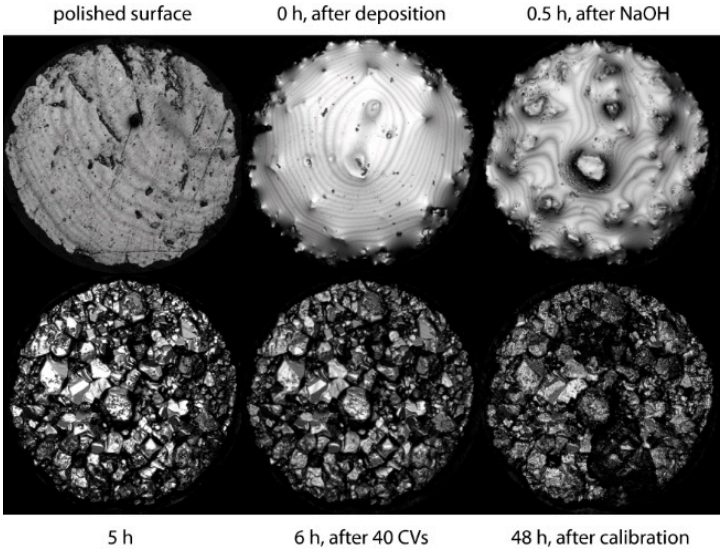


Figure 11. Change of gold amalgam electrode surface over time (100-µm diameter).

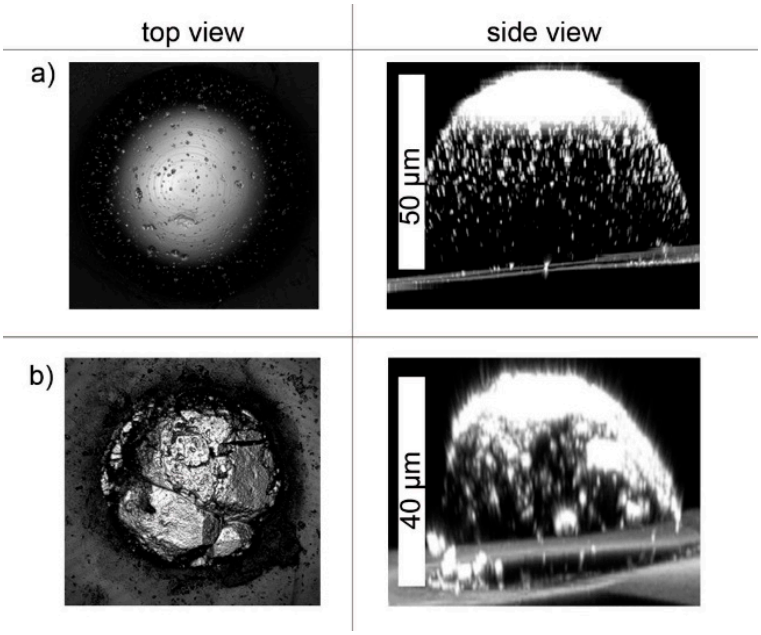


Figure 12. Large conical mercury deposition (**a**) immediately after plating and (**b**) after calibration and nine days of consecutive CSV measurements.

From both observations, it can be concluded that the GAME surface undergoes significant changes during maturation and application. Hereby, flat and conical electrode geometries differ.

4. Discussion

4.1. Calibration

Zhang et al. gave an overview on sulfide concentrations in waste streams that require emission control [5]. The span ranges from 80 µM to 2.2 mM sulfide. Facing this range, the present gold amalgam microelectrode provides a suitable detection range from 50 µM–1.5 mM. The range of CSV was obtained by using the settings already suggested by Luther et al. [8].

Wastewater contains metal ions, which may interfere with the GAME CSV-method, but the allowed concentrations are typically regulated by legislation. In German municipal wastewater, for instance, the legal limit for copper and zinc entering the wastewater stream is 8 and 15 µM, respectively (German discharge requirement regulation AbwV, Supplement 39). If these threshold values are met, little interference with the described GAME CSV sulfide measurement is expected in real municipal wastewater. In contrast, industrial wastewater may contain much higher concentrations such as 7 mM copper or 9 mM zinc [32]. Thus, if the GAME CSV method is intended for tracing sulfide or metals in industrial wastewater treatment processes, the method would require further adjustment. To achieve this, the adjustable accumulation time holds great potential. A control circuit could be set up, which increases the accumulation time in response to sulfide concentrations. This approach could result in a complete linear response ranging from below 50 µM and exceeding 2 mM with a single electrode. In addition, a separate anodic stripping procedure might allow the parallel determination of manganese, copper, iron, or zinc if desired.

At high sulfide concentration, saturation effects became visible. This might be due to two effects. First, it might be a saturation response as seen in the accumulated time experiment. Second, it might be due to the conversion of sulfide to polysulfide anions [10]. Since the sulfide concentration was raised during calibration, new reductive peaks became visible (Figure 5). Such peaks have been reported to originate from a two-step reduction of polysulfides [19].

$$HgS_x + 2\,e^- \rightarrow Hg + {S^{2-}}_x \quad (4)$$

$${S^{2-}}_x + xH^+ + (2x-2)\,e^- \rightarrow xHS^- \quad (5)$$

When sulfide was gradually removed from the system by nitrogen sparging during CSV, sulfide peaks as well as the potential polysulfide peaks disappeared (data not shown). During microbial sulfide production, polysulfide peaks were less emphasized when compared to the calibration at similar sulfide levels. In conclusion, these effects during calibration might result in the overestimation of sulfide concentrations during experiments and should be handled with care.

4.2. Microbial Sulfide Emissions

Ramm and Bella determined the rate of sulfide emission in media representing the benthic environment and reviewed rates in several other systems [33]. Their complex algae media contained 1.125 g/L soluble organic carbon and between 2–10 mM sulfate. At 20 °C, they determined a sulfide formation rate of 13–91 µM h^{-1} L^{-1}. Not surprisingly, they found that the rate depends on sulfate and organic content. Given their findings, the ~ 5 µM h^{-1} of sulfide emission in AWW 1 appear low but can be explained by the low initial sulfate content.

Since hydrogen sulfide has been found to be involved in cell signaling, more attention has been paid to the biochemical interconversion of cysteine and hydrogen sulfide [34–36]. Unfortunately, up to now, only the present study appears to give insights into cysteine-based sulfide emission, particularly for wastewater-like systems.

The calculation of sulfide emissions in artificial wastewater and real wastewater is of relevance for microbial fuel cell (MFC) research. For MFC studies, it is important to know how many electrons from a substrate will be used to reduce the anode [37]. The ratio between charge potentially available from the substrate and the reductive charge measured at the anode is called coulombic efficiency (CE).

While 100 µM sulfide emissions in AWW 1 have a negligible effect on the electrode balance of 10 mM substrate during anodic respiration, this is different in AWW 2. The emission of almost 2 mM sulfide will represent a significant electron sink. This should be considered when calculating the coulombic efficiencies and balancing a bio-electrochemical system in such media.

4.3. Potential Improvements for GAME Production

In polarography, the self-renewal of the Hanging Drop Mercury Electrode (HDME) is a desired feature to provide a new smooth and uncontaminated electrode surface. For environmental applications, however, the loss of a mercury drop during plating is rather disadvantageous. Based on the variable mercury plating results, we hypothesize that excess mercury eventually gets lost during the further electrode handling, which leaves behind an undefined surface structure (Figure 13).

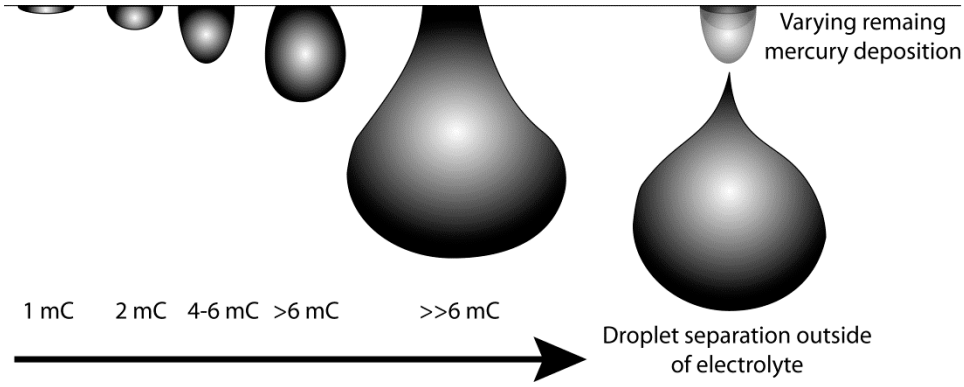


Figure 13. Hypothetical mercury droplet loss after excess plating on a gold electrode surrounded by epoxy resin.

To create a more reliable electrode formation, it is suggested to limit the absolute amount of mercury instead of the deposition time. A 100-µm gold electrode appeared unlikely to hold a deposition higher than 3–6 µg Hg, which corresponded to a deposition charge of 3–6 mC. The method should be adjusted accordingly by limiting the plating charge.

Stability could be increased by slowing down the deposition process, which results in deeper penetration of mercury into the gold wire. If the disequilibrium of a separate gold and amalgam phase was undesired in the first place, a homogeneous silver-mercury (dental amalgam) was suggested [38]. Furthermore, the beneficial micro-size fabrication could be altered more tediously.

4.4. GAME Maturation and Aging

It was found that the GAME surface undergoes roughening and recrystallisation during measurements. The reason is that the gold and amalgam phases are not in equilibrium. Changes in amalgam surface structures have been of special interest, e.g., due to the popularity in dental applications. Early research involving visual evidence for amalgam corrosion was provided by Matono and Fusayama [39]. Others have observed the formation of dendritic-like AuHg structures of mercury in contact with gold using scanning electron microscopy (SEM) and X-ray photoelectron spectroscopy [40]. Despite the similar interest in amalgams for electroanalytical applications, surfaces have been less subject to visual analysis. Hou et al. provide insights into the amalgam formation on thin gold films due to mercury sorption by showing beautiful SEM images [41], which is similar to earlier scanning tunneling microscopy studies from George et al. [42]. Nevertheless, the GAME provides a solid underlying gold body and higher amounts of deposited mercury, which shows larger crystal structures and complex interactions shaping the desired surfaces. Amalgam crystals of similar dimensions have been observed for Ag-Sn-Cu alloys, but not for gold [43]. Thus, the present study

provides the first microscopic insights on the shapes and changes of gold amalgam microelectrode surface structures.

Before using the GAME for analytical purposes, the amalgam crystal structure is recommended to mature, dependent on layer thickness. We found a thin layer of mercury to crystallize within 6 h. This is lower when compared to previous findings. An electrode signal stabilized after maturation of at least 12 h [44] and solidification of 1-µm mercury film on silver required a period of more than 24 h [45].

5. Conclusions

Concerning the central question of this work, we conclude that the use of gold amalgam electrodes in the intended chemical environment is a feasible approach. Cathodic stripping voltammetry was successfully adapted to determine sulfide concentrations in artificial wastewater, which is a defined medium typically used in microbial fuel cell experiments. Gold amalgam microelectrodes with a 100-µm diameter were fabricated and were capable of detecting sulfide concentrations between 22–1500 µM. The calibrated solid-state electrodes remained stable for at least six days. They were applied to trace microbial sulfide formation in two different types of artificial wastewater. Artificial wastewater 1 contained a total of 200 µM sulfur components. For this medium, we observed a sulfur conversion of approximately 50% after more than 40 h at a maximum rate of ~4.3 ± 0.5 µM h^{-1}. In contrast, artificial wastewater type 2 contained a total of 2212 µM sulfur components and we observed a conversion between 75% to almost 100% after 30 h at a maximum rate of 165 µM h^{-1}.

This work carefully assessed a previously used chronoamperometric mercury plating method for fabricating gold amalgam microelectrodes. We found that this procedure is likely to result in a variable mercury plating and, subsequently, varying electrode surfaces, which affect the calibration and application of these electrodes for cathodic stripping voltammetry. We suggest terminating the mercury plating after a certain deposition charge has been reached, rather than using a defined plating time. This may result in more reproducible plating and, thus, reproducible electrode performance.

Confocal laser scanning was used to assure the microelectrode surface quality. For the first time to our knowledge, gold electrode surface changes during amalgam crystallization and aging have been observed in detail for varying mercury depositions. Thin mercury platings appear to form stable crystal structures within 6 h after deposition. This suggests that the electrodes are ready for use more quickly than previously reported.

The future objective is to adapt gold amalgam microelectrodes for continuous real-time sulfide measurement in real wastewater, for which this study has provided the base. A performance comparison would be required to evaluate the practical advantages of the gold amalgam microelectrodes compared to other techniques and its potential for later commercialization. This would not only include tests for stability, linear range, and the bill of materials but also an analysis of the "expected purchase price" suggested by Wilson et al. [46].

Supplementary Materials: The following are available online at http://www.mdpi.com/2227-9040/8/3/49/s1. Figure S1: Photographic electrode images, Figure S2: Methylene blue calibration images, Figure S3: Cathodic sweeps in artificial wastewater and in phosphate buffer.

Author Contributions: J.M.S.A. designed and performed the experiments in the context of his PhD-Project [47]. J.M.S.A. wrote the manuscript in consultation with U.S. In addition, U.S. supervised the project. All authors have read and agreed to the published version of the manuscript.

Funding: This research received no external funding.

Acknowledgments: J.M.S.A. acknowledges the financial support from the German Academic Scholarship Foundation. We acknowledge support by the German Research Foundation and the Open Access Publication Funds of the Technische Universität Braunschweig.

Conflicts of Interest: The authors declare no conflict of interest.

References

1. Nielson, A.R.H.; Vollertsen, J.; Hvitved-Jacobsen, T. *Sewer Processes: Microbial and Chemical Process Engineering of Sewer Networks*, 2nd ed.; Crc Pr Inc: Aalborg, Denmark, 2013.
2. Jensen, H.S. *Hydrogen Sulfide Induced Concrete Corrosion of Sewer Networks*; Aalborg University: Aalborg, Denmark, 2009.
3. Hao, T.; Xiang, P.-Y.; Mackey, H.R.; Chi, K.; Lu, H.; Chui, H.-K.; Van Loosdrecht, M.C.M.; Chen, G. A review of biological sulfate conversions in wastewater treatment. *Water Res.* **2014**, *65*, 1–21. [CrossRef] [PubMed]
4. Takagi, H.; Ohtsu, I. L-Cysteine metabolism and fermentation in microorganisms. In *Advances in Biochemical Engineering/Biotechnology*; Springer Science and Business Media Deutschland GmbH: Berlin, Germany, 2017. [CrossRef]
5. Zhang, L.; De Schryver, P.; De Gusseme, B.; De Muynck, W.; Boon, N.; Verstraete, W. Chemical and biological technologies for hydrogen sulfide emission control in sewer systems: A review. *Water Res.* **2008**, *42*, 1–12. [CrossRef] [PubMed]
6. Ganigué, R.; Gutierrez, O.; Rootsey, R.; Yuan, Z. Chemical dosing for sulfide control in Australia: An industry survey. *Water Res.* **2011**, *45*, 6564–6574. [CrossRef]
7. Lawrence, N. Analytical strategies for the detection of sulfide: A review. *Talanta* **2000**, *52*, 771–784. [CrossRef]
8. Luther, G.W.; Glazer, B.T.; Ma, S.; Trouwborst, R.E.; Moore, T.S.; Metzger, E.; Kraiya, C.; Waite, T.J.; Druschel, G.; Sundby, B.; et al. Use of voltammetric solid-state (micro)electrodes for studying biogeochemical processes: Laboratory measurements to real time measurements with an in situ electrochemical analyzer (ISEA). *Mar. Chem.* **2008**, *108*, 221–235. [CrossRef]
9. Luther, G.W.; Findlay, A.J.; Macdonald, D.J.; Owings, S.M.; Hanson, T.E.; Beinart, R.A.; Girguis, P.R. Thermodynamics and Kinetics of Sulfide Oxidation by Oxygen: A Look at Inorganically Controlled Reactions and Biologically Mediated Processes in the Environment. *Front. Microbiol.* **2011**, *2*, 1–9. [CrossRef]
10. Luther, G.W., III; Glazer, B.T.; Hohmann, L.; Popp, J.I.; Taillefert, M.; Rozan, T.F.; Brendel, P.J.; Theberge, S.M.; Nuzzio, D.B. Sulfur speciation monitored in situ with solid state gold amalgam voltammetric microelectrodes: Polysulfides as a special case in sediments, microbial mats and hydrothermal vent waters. *J. Environ. Monit.* **2001**, *3*, 61–66. [CrossRef]
11. Luther, G.W.; Ferdelman, T.G. Voltammetric characterization of iron(II) sulfide complexes in laboratory solutions and in marine waters and porewaters. *Environ. Sci. Technol.* **1993**, *27*, 1154–1163. [CrossRef]
12. Van den Berg, M.G. Adsorptive cathodic stripping voltammetry of trace elements in sea water. *Analyst* **1989**, *114*, 1527. [CrossRef]
13. Schröder, H. Surfactants: Non-biodegradable, significant pollutants in sewage treatment plant effluents. *J. Chromatogr. A* **1993**, *647*, 219–234. [CrossRef]
14. Sedlak, D.L.; Phinney, J.T.; Bedsworth, W.W. Strongly Complexed Cu and Ni in Wastewater Effluents and Surface Runoff. *Environ. Sci. Technol.* **1997**, *31*, 3010–3016. [CrossRef]
15. Baudler, A.; Riedl, S.; Schröder, U. Long-Term Performance of Primary and Secondary Electroactive Biofilms Using Layered Corrugated Carbon Electrodes. *Front. Energy Res.* **2014**, *2*, 1–6. [CrossRef]
16. Luther, G.W.; Swartz, C.B.; Ullman, W.J. Direct determination of iodide in seawater by cathodic stripping square wave voltammetry. *Anal. Chem.* **1988**, *60*, 1721–1724. [CrossRef]
17. Brendel, P.J.; Luther, G.W. Development of a Gold Amalgam Voltammetric Microelectrode for the Determination of Dissolved Fe, Mn, O_2, and S(-II) in Porewaters of Marine and Freshwater Sediments. *Environ. Sci. Technol.* **1995**, *29*, 751–761. [CrossRef] [PubMed]
18. Bard, A.J.; Faulkner, L.R.; Swain, E.; Robey, C. *Electrochemical Methods: Fundamentals and Applications*, 2nd ed.; Harris, D., Swain, E., Robey, C., Aiello, E., Eds.; JOHN WILEY & SONS, INC.: New York, NY, USA, 2001.
19. Glazer, B.T.; Cary, S.C.; Hohmann, L.; Luther, G.W. In Situ Sulfur Speciation Using Au/Hg Microelectrodes as an Aid to Microbial Characterization of an Intertidal Salt Marsh Microbial Mat. *ACS Symp. Ser.* **2002**, *811*, 283–304. [CrossRef]
20. Ma, S.; Luther, G.W.; Keller, J.; Madison, A.S.; Metzger, E.; Emerson, D.; Megonigal, J.P. Solid-State Au/Hg Microelectrode for the Investigation of Fe and Mn Cycling in a Freshwater Wetland: Implications for Methane Production. *Electroanalysis* **2008**, *20*, 233–239. [CrossRef]
21. Bobrowski, A.; Królicka, A. Renewable silver amalgam film electrodes in electrochemical stripping analysis—A review. *J. Solid State Electrochem.* **2016**, *20*, 3217–3228. [CrossRef]

22. Hamann, C.H.; Vielstich, W. *Elektrochemie*; Wiley-VCH: Weinheim, Germany, 2005.
23. Hughes, M.N.; Centelles, M.N.; Moore, K.P. Making and working with hydrogen sulfide. *Free. Radic. Boil. Med.* **2009**, *47*, 1346–1353. [CrossRef] [PubMed]
24. Cline, J. Spectrophotometric determination of hydrogen sulfide in natural waters. *Limnol. Oceanogr.* **1969**, *14*, 454–458. [CrossRef]
25. Riedl, S.; Brown, R.K.; Klöckner, S.; Huber, K.J.; Bunk, B.; Overmann, J.; Schröder, U. Successive Conditioning in Complex Artificial Wastewater Increases the Performance of Electrochemically Active Biofilms Treating Real Wastewater. *Chem. Electro. Chem.* **2017**, *4*, 3081–3090. [CrossRef]
26. Baudler, A.; Schmidt, I.; Langner, M.; Duan, G.; Schröder, U. Does it have to be carbon? Metal anodes in microbial fuel cells and related bioelectrochemical systems. *Energy Environ. Sci.* **2015**, *8*, 2048–2055. [CrossRef]
27. Kim, J.R.; Min, B.; Logan, B.E. Evaluation of procedures to acclimate a microbial fuel cell for electricity production. *Appl. Microbiol. Biotechnol.* **2005**, *68*, 23–30. [CrossRef] [PubMed]
28. Bialek, K.; Kim, J.; Lee, C.; Collins, G.; Mahony, T.; O'Flaherty, V. Quantitative and qualitative analyses of methanogenic community development in high-rate anaerobic bioreactors. *Water Res.* **2011**, *45*, 1298–1308. [CrossRef] [PubMed]
29. Schindelin, J.; Arganda-Carreras, I.; Frise, E.; Kaynig, V.; Longair, M.; Pietzsch, T.; Preibisch, S.; Rueden, C.; Saalfeld, S.; Schmid, B.; et al. Fiji: An open-source platform for biological-image analysis. *Nat. Methods* **2012**, *9*, 676–682. [CrossRef] [PubMed]
30. Frankel, J.J. Notes on gold amalgam crystals. *J. Chem. Metall. Min. Soc. S. Afr.* **1956**, *12*, 451–456.
31. Wu, F.; Qi, S. Global View of Engineering Geology and the Environment. In Proceedings of the International Symposium and 9th Asian Regional Conference of IAEG BT—International Symposium and 9th Asian Regional Conference of IAEG and the Environment, Beijing, China, 24–25 September 2013.
32. Azimi, A.; Azari, A.; Rezakazemi, M.; Ansarpour, M. Removal of Heavy Metals from Industrial Wastewaters: A Review. *Chem. Biomol. Eng. Rev.* **2017**, *4*, 37–59. [CrossRef]
33. Ramm, A.E.; Bella, D.A. Sulfide production in anaerobic microcosms. *Limnol. Oceanogr.* **1974**, *19*, 110–118. [CrossRef]
34. Kabil, O.; Banerjee, R. Redox Biochemistry of Hydrogen Sulfide. *J. Boil. Chem.* **2010**, *285*, 21903–21907. [CrossRef]
35. Benavides, G.A.; Squadrito, G.L.; Mills, R.W.; Patel, H.D.; Isbell, T.S.; Patel, R.P.; Darley-Usmar, V.; Doeller, J.E.; Kraus, D.W. Hydrogen sulfide mediates the vasoactivity of garlic. *Proc. Natl. Acad. Sci. USA* **2007**, *104*, 17977–17982. [CrossRef]
36. Goubern, M.; Andriamihaja, M.; Nübel, T.; Blachier, F.; Bouillaud, F. Sulfide, the first inorganic substrate for human cells. *FASEB J.* **2007**, *21*, 1699–1706. [CrossRef]
37. Zhao, F.; Slade, R.C.T.; Varcoe, J.R. Techniques for the study and development of microbial fuel cells: An electrochemical perspective. *Chem. Soc. Rev.* **2009**, *38*, 1926–1939. [CrossRef] [PubMed]
38. Mikkelsen, Ø.; Schrøder, K.H. Amalgam Electrodes for Electroanalysis. *Electroanalysis* **2003**, *15*, 679–687. [CrossRef]
39. Matono, R.; Fusayama, T. Corrosion of amalgam in contact with gold. *J. Prosthet. Dent.* **1972**, *28*, 170–178. [CrossRef]
40. Bergman, B.; Bergman, M.; Helander, H. Appearance of surfaces of dental amalgam in contact with gold: An in vivo study. *Acta Odontol. Scand.* **1982**, *40*, 325–332. [CrossRef]
41. Hou, T.; Chen, M.; Greene, G.W.; Horn, R.G. Mercury Vapor Sorption and Amalgamation with a Thin Gold Film. *ACS Appl. Mater. Interfaces* **2015**, *7*, 23172–23181. [CrossRef]
42. George, M.A.; Glaunsinger, W.S.; Thundat, T.; Lindsay, S.M. Investigation of mercury adsorption on gold films by STM. *J. Microsc.* **1988**, *152*, 703–713. [CrossRef]
43. Koike, M.; Ferracane, J.L.; Fujii, H.; Okabe, T. Evaluation of the amalgamation reaction of experimental Ag-Sn-Cu alloys containing Pd using a mercury plating technique. *Dent. Mater. J.* **2003**, *22*, 280–291. [CrossRef]
44. O'Shea, T.J.; Lunte, S.M. Selective detection of free thiols by capillary electrophoresis-electrochemistry using a gold/mercury amalgam microelectrode. *Anal. Chem.* **1993**, *65*, 247–250. [CrossRef]
45. Ostapczuk, P.; Kublik, Z. Silver based mercury film electrode. *J. Electroanal. Chem. Interfacial Electrochem.* **1978**, *93*, 195–212. [CrossRef]

46. Wilson, D.J.; Kumar, A.A.; Mace, C.R. Overreliance on Cost Reduction as a Featured Element of Sensor Design. *ACS Sens.* **2019**, *4*, 1120–1125. [CrossRef]
47. Andrich, J.M.S. Down Under—Aspects of Microbial Fuel Cell's Sewer Implementation. Ph.D. Thesis, Technische Universität Braunschweig, Braunschweig, Germany, 2017.



© 2020 by the authors. Licensee MDPI, Basel, Switzerland. This article is an open access article distributed under the terms and conditions of the Creative Commons Attribution (CC BY) license (http://creativecommons.org/licenses/by/4.0/).